XL CILAMCE
IBERO-LATIN AMERICAN CONGRESS ON COMPUTATIONAL METHODS IN ENGINEERING
NOVEMBER 11-14, 2019
Praiamar Natal Hotel & Convention
Natal, RN-BRAZIL

FATIGUE ANALYSIS OF THE GROUTED CONNECTION OF AN OFFSHORE WIND TURBINE

Fellipe A. Gomes
Gilberto B. Ellwanger
José R. M. de Sousa
fellipe.gomes@coc.ufrj.br
gbe@coc.ufrj.br
jrenato@laceo.coppe.ufrj.br
Department of Civil Engineering, Federal University of Rio de Janeiro
Av. Athos da Silveira Ramos, 149, 21941-909, Ilha do Fundão, Rio de Janeiro, Brazil

Abstract. Due to technological advances, Offshore Wind Turbines (OWT) have proven to be a viable investment alternative in Brazil. However, unlike offshore structures originally developed for the oil and gas industry, OWT support structures are subject to large bending moments due to the wind and wave loads on the structure. One of the critical regions of an OWT is the structural connection between the superstructure and its foundation. This is commonly performed through a cylindrical joint filled with high-performance grout, made by a metal transition piece that transfers the stresses to foundation through the grout. The present article aims to evaluate the structural fatigue, under operational and parked condition, of the grouted connection of a monopile foundation in water depth of 20 meters in cohesive soil, using SIMA-RIFLEX and TurbSim software. The soil-structure interaction is simulated applying p-y curves proposed by ANSI / API-RP-2GEO (2011) and DNVGL-ST-0126 (2016). Fatigue damage is analyzed by applying the Rainflow Counting and S-N curve proposed by DNVGL-ST-C502 (2018) for the grout. It was identified that more severe environmental conditions generate greater damages, and this behavior is strongly influenced by the rated speed of the turbine and natural frequency of the structure.

Keywords: Offshore wind turbine, Fatigue, Grouted connection, Monopile.

1 Introduction

Brazil already has 583 onshore wind farms in operation, totaling 15 GW of installed capacity, according to ABEE [1]. However, the Brazilian wind market goes way beyond this capacity. The total onshore wind resources reach 143.5 GW, at a height of 50 meters (AMARANTE et al. [2]), showing that there is still much to be explored. However, the capacity yet to be developed at sea draws more attention. Brazil presents offshore wind resources in the order of 1.3TW, in shallow water, with depths up to 50 meters, which is almost nine times bigger than the onshore wind resources (Silva et al. [3]). In addition to this, offshore wind resources exhibit great complementarity between the wind regimes of the North-Northeast region and the Brazilian water resources as stated by Silva et al. [3], what in the long run will come handy, since the wind power source would complement the electricity supply in periods of low production of hydroelectric sources.

Given the capacity of Brazil to develop in the offshore wind sector, it is imperative to develop studies in the area. These studies involve not only analysis of wind resources, but also analysis of the wind turbine support structures, which may account for 20-25% of the cost of offshore wind farms (Srikanth et al. [4]). In Europe, the most widely-used support structure is the monopile foundation, with a market share of approximately 82%, according to EWEA [5]. This type of foundation consists of a pile with a diameter that can go up to 9 meters and a longitudinal length ranging from 21-85 meters, being embedded up to 40 meters below the seabed (NEGRO et al. [6]). Once the monopile is driven into the soil, the connection between the foundation pile and the tower is achieved through a cylindrical joint, filled with high-performance grout, made by a metal transition piece that transfers the stresses to foundation through the grout.

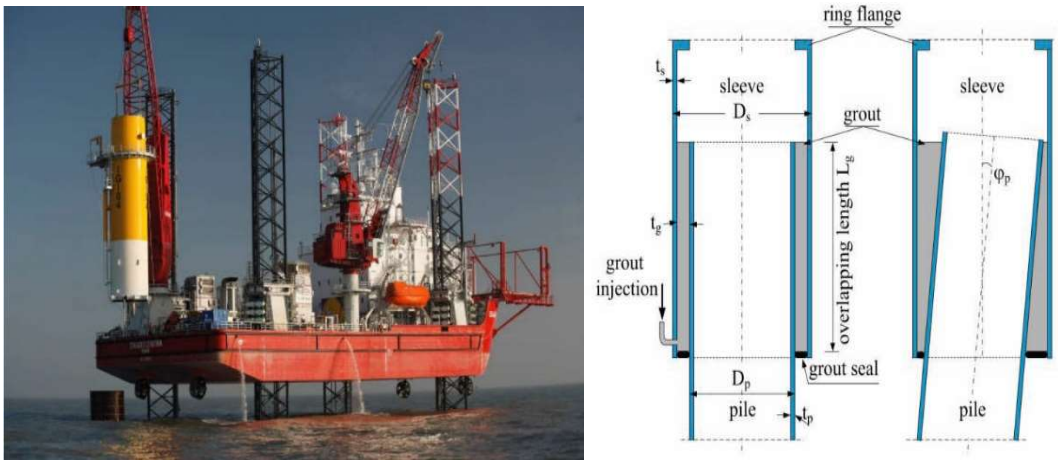

Figure 1. Installation of the transition piece to form the grouted connection (Vattenfall [7] and Schaumann et al. [8]).

The study of this type of connection dates back to the 1970s when its fatigue and strength capacity was analyzed by Billington and Lewis [9]. At that time, these connections were used in marine structures for the oil and gas industries, in connections between jacket structure and its piles, however, it had smaller dimensions, around 1 to 3 meters in diameter, compared with the size of the structures currently being used in the offshore wind industry. Due to its successful application in oil and gas structures, the grouted connection was introduced in the offshore wind sector. Though, it was noted that the OWTs were exposed to large bending moments (Lotsberg et al. [10]), consequently, several offshore wind farms (Horns Rev 1, Kentish Flats and Belwind) reported insufficient capacity of the connection, leading to the settlement of the transition piece along the monopile (Dallyn et al. [11]).

As a consequence of these failures, a joint industry project (Lotsberg et al. [10]) was carried out to investigate the capacity of these connection, resulting in analytical design equations that were later adopted by DNVGL-ST-0126 [12]. In that project, two different design procedures were recommended in order to increase its capacity, one for conical shaped connections (Fig. 2) and another for cylindrical

shaped connections with shear keys (Fig. 3). Shear keys are weld bead that are placed around the outer side of the pile and around the inside of the transition piece in the hoop direction, aimed at restraining the sliding of the transition piece along the pile (Schaumann et al. [13]).

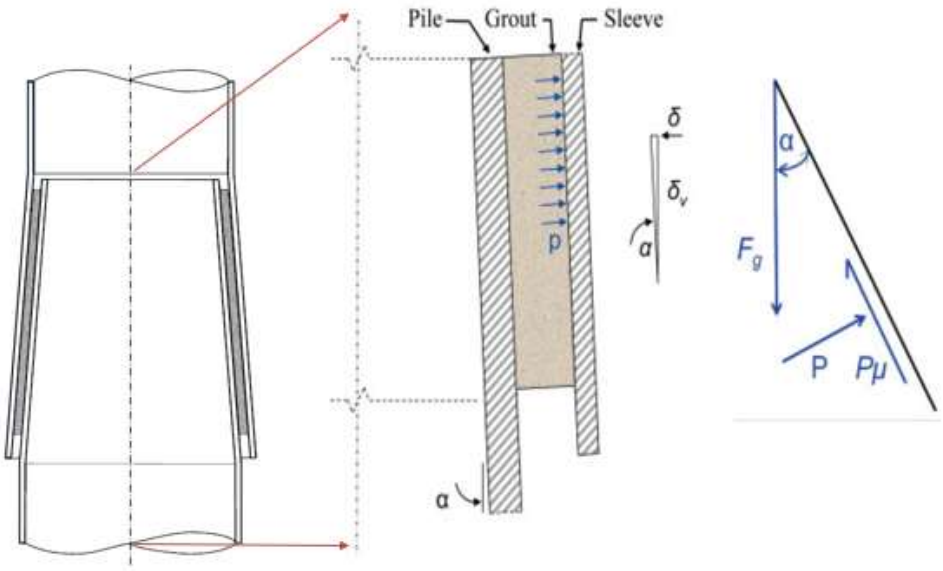

Figure 2. Conical shaped grouted connection (Lotsberg et al. [10] and DNVGL-RP-0419 [14]).

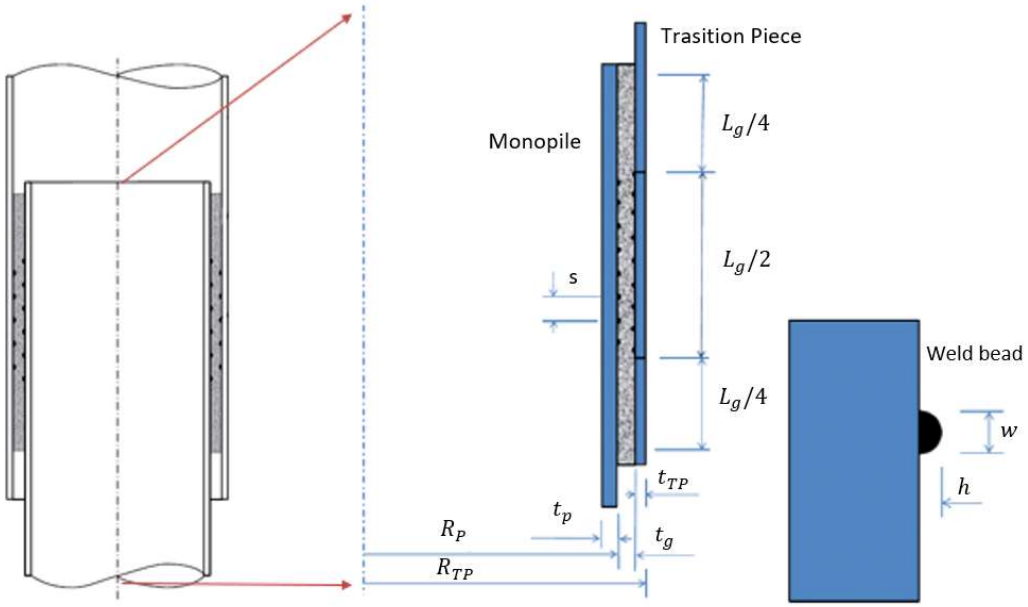

Figure 3. Cylindrical shaped connection with shear keys (DNVGL-ST-0126 [12] and DNVGL-RP-0419 [14]).

As a result of stochastic wind and wave loads, OWTs are subjected to 10^9 load cycle over its life time, which makes the fatigue analysis of these connections extremely significant. Due to this, in the present work, the fatigue behavior of these two different grouted joints subjected to predominant bending action are assessed. Moreover, a sensitive analysis of the high-performance grout is conducted on how the mean cyclic load, compressive resistance of grout and number of shear connectors affects

the fatigue life of both connections. The representative load cases were based on the southeast region of Brazil, and the software tool SIMA by MARINTEK is used in combination with in-house spreadsheet to obtain estimates of the fatigue damage.

The paper is organized as follows: First, a description of the wind turbine model and support structures with grouted connection is given. Further, it is provided the environmental conditions and wind and wave model is presented. After, the mechanical behavior and the procedure for calculation of the fatigue damage are described. Simulations results are then presented along with discussion and in the end, a conclusion.

2 Reference turbine model

2.1 NREL 5MW baseline offshore wind turbine

The turbine model chosen was based on the 5MW Baseline Wind Turbine from the National Renewable Energy Laboratory (NREL) with a rated power of 5MW (Table 1). This turbine was based on Senvion 5MW prototype and is considered representative of sea-based turbines. For additional details the reader may refer to Jonkman et al. [15].

Table 1. NREL baseline wind turbine (Jonkman et al. [15]).

Rating	5MW
Rotor orientation	Upwind; 3 blades
Control	Variable speed, collective pitch
Rotor and hub diameter	126m; 3m
Hub height	90m
Cut-in, rated, cut-out wind speed	3m/s;11,4m/s;25m/s
Cut-in, rated rotor speed	6,9rpm; 12,1rpm

2.2 Support structure with grouted connection

In order to include the transition piece, the reference support structure from Jonkman et al. [15] was adapted based on the information provided in Damgaard et al. [16], which presents the geometry properties from one monopile support structure installed in the North Sea for a Vestas V90-3.0MW wind turbine. The final design is shown in Fig. 4. Further details for both conical and cylindrical shaped grouted connections are provided in Table 2. Symbols are according to Fig. 2 and Fig. 3.

Table 2. Geometry parameters of the grouted connection

Geometry	Symbol	Unit	Connection shape	
			Conical	Cylindrical with shear key
Number of shear key (total)	[-]	[-]	[-]	27
Cone angle	(α)	°	1	[-]
Length of grouted section	(L_g)	m	9.1	9.1
Pile outer radius	(R_p)	m	3	3
Transition piece outer radius	(R_{tp})	m	3.11	3.11
Thickness of transition piece	(t_s)	m	0.06	0.06
Wall thickness of pile	(t_p)	m	0.06	0.06
Thickness of grout	(t_g)	m	0.05	0.05

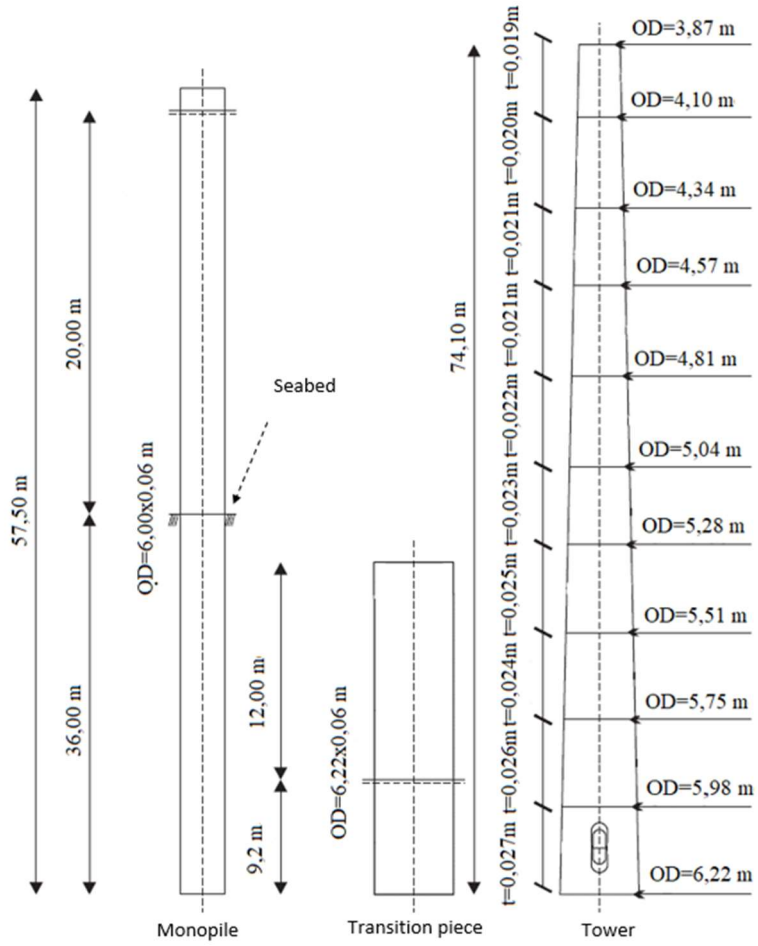

Figure 4. Adapted support structure (Adapted from Damgaard et al. [16]).

The support structure and the NREL 5MW wind turbine were modeled in RIFLEX software [17] (Fig. 5), which is a coupled non-linear aero-hydro-servo-elastic simulation tool. Tower, grouted connection and monopile were modeled as axisymmetric pipe with material properties according to Table 3. Moreover, following Velarde and Bachynski [18], the model includes Rayleigh damping, equivalent to a damping ratio of $\zeta = 2\%$.

Table 3. Material properties

Material	Steel	Grout	Unit
Young's modulus	210.0	53.0	GPa
Poisson's ratio	0.3	0.19	[-]
Grout to steel interface friction coefficient	0.4		μ
Density	8.500	2.512	Kg/m3
Compressive strength	[-]	80	MPa
Yield strength	235	[-]	MPa

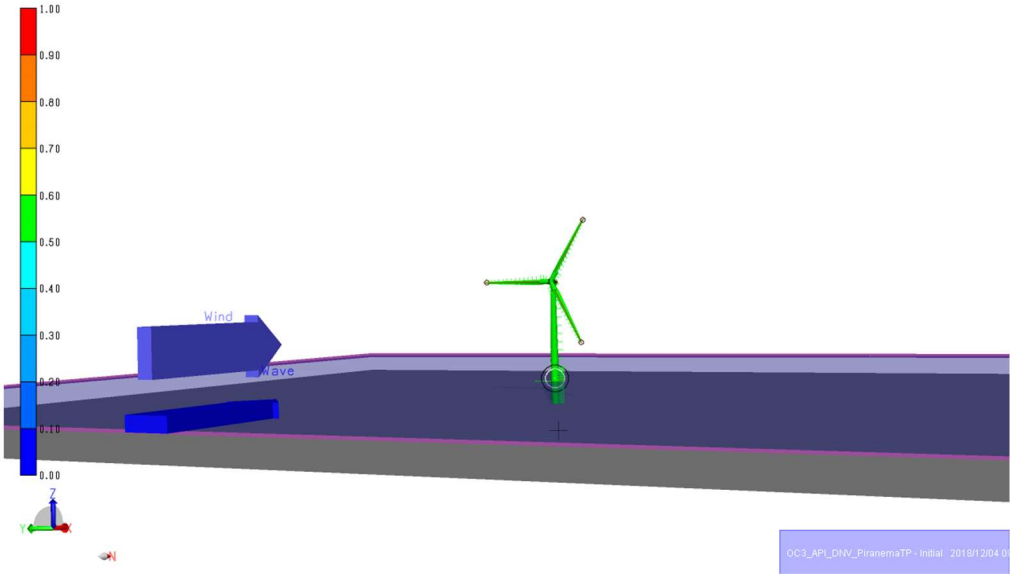

Figure 5. NREL 5MW wind turbine in RIFLEX (Gomes [19]).

2.3 Soil-structure interaction

In this study, for simplicity, the nonlinear Winkler model associated with p-y curves recommended in ANSI/API-RP-2GEO [20] and DNVGL-ST-0126 [12] was used. The use of this methodology was recommended for cohesive soils based on Matlock [21], Reese and Welch [22] and Dunnavant and O'neill [23]. Although these models were designed only for piles up to 2 meters in diameter (monopile has 6 meters in diameter), this methodology is well accepted and similar procedure was implemented in other works, such as Bisoi and Hadar [24], Schafhirt et al. [25] and Smilden [26].

According to Winkler's model, the monopile is assumed to behave as a Euler-Bernoulli beam and is discretized into elements that are associated with decoupled soil springs, equidistant from each other, representing the lateral stiffness of the soil against the lateral pile displacement. The spring response "p" per unit length, applied by the soil, depends on the soil properties and magnitude of the displacement "y" of the structure (Fig. 5). For the analysis, clay soil with 3 different undrained shear strength (s_u= 10 KPa, s_u= 20 KPa e s_u= 50 KPa) and effective unit weight (γ_{sub}) of 8.5 kN/m^2 were used. The pile has an embedment length of 36 meters as per Fig 4.

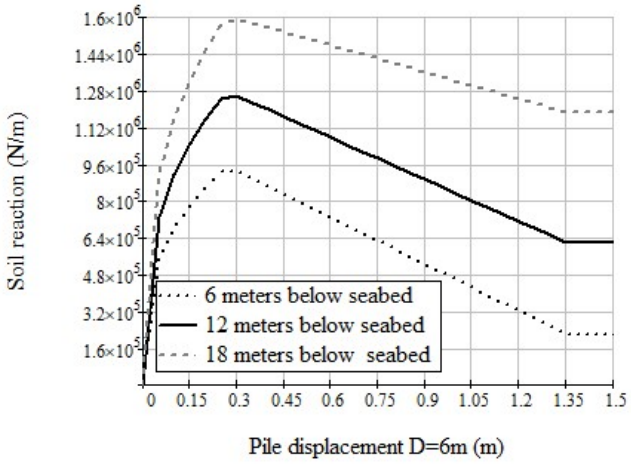

Figure 6. DNV and based p-y curve (Gomes [18]).

2.4 Forcing frequency 1P and 3P

The support structure of an OWT is highly susceptible to different dynamic loads, some of them are inherent to its own operation. Nevertheless, these operational loads act on the support structure with known frequencies, the so called 1P and 3P frequencies, which are associated with the shadowing effect each time a blade passes the tower and mass imbalances in the blade. 1P is the rotor revolution frequency and 3P is the blade passing frequency for a 3 bladed wind turbine. In the case of the NREL 5MW baseline, the 1P ranges from 5 to 8.6 seconds (0.12-0.20 Hz) and the 3P ranges from 1.65 to 2.86 seconds (0.35-0.61 Hz), according to Jonkman et al. [15]. This change in the rotational speed of the rotor is due to pitch control of the blades that changes its angle of attack according to wind speeds from 11.4m/s (rated wind speed) up to 25m/s (cut-out wind speed).

This pitch control of the blades has two main consequences, optimization of energy yielding and reduction of the thrust force, which is a force that acts normal to the plane of rotation of the blade (Gasch and Twele [27]). The thrust reduction has beneficial effect on the support structure, leading to lower bending moments at the base. Figure 7 shows preliminare results of simulations conducted with varying wind speeds, and it is possible to identifie that higher wind speeds (from 11 m/s) yeilds lower bending moments on the structure as a consequence of lower thrusts forces, as stated by Gasch and Twele [27].

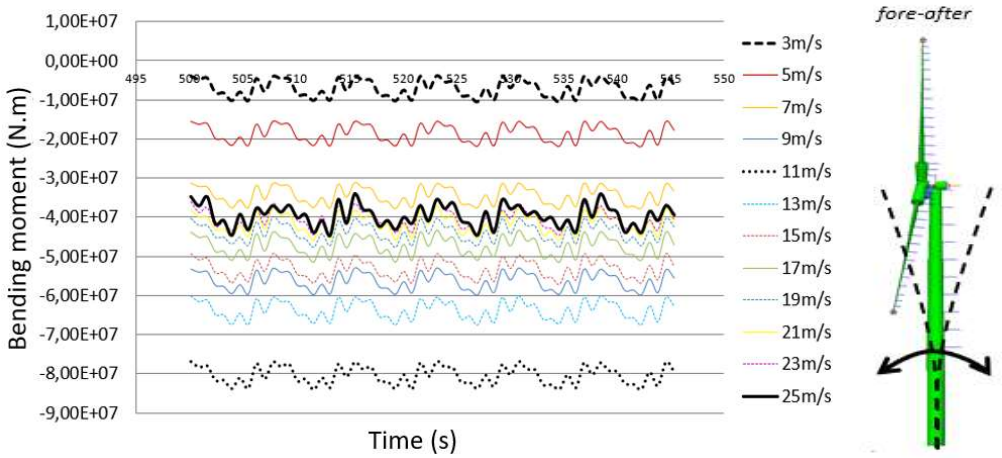

Figure 7. Left: bending moment on the base; right: fore-after vibration mode (Gomes [19]).

2.5 Natural frequency

The natural frequency of the lowest mode of the OWT adopted in this study, in the fore-after direction, is shown in Table 4. It is of main importance to note changes in the natural frequency as a consequence of soil properties changes, which, depending on the forcing loads frequencies, may lead to dynamic response amplification.

Table 4. Natural frequency

Undrained shear strength (s_u)	$f_{0,n}$ (Hz)	T (s)
10 KPa	0.216	4.63
20 KPa	0.221	4.52
50 KPa	0.235	4.25

3 Design load analysis

In the design of OWT´s, the fatigue analysis should be conducted for a large set of cases in accordance with a scatter diagram, for a specified site, where the most frequent environmental conditions are identified (DNVGL-ST-0437 [28]). However, for simplicity, two design load cases (DLC) were chosen taking into consideration different design situation: operational and parked (DLC 1.2 and DLC 6.4, in agreement with IEC61400-3 [29], respectively).

During operational design situation, the turbine is converting kinetic energy from the wind into mechanical power. Thus, the wind speed that passes the turbine is in between 3m/s and 25m/s, as specified in Table 1. However, when it is in parked or idling design situation, the wind speed that passes the turbine is either under 3m/s or over 25m/s. For both cases, the wind turbulence intensity was taken according to IEC IIB category, as provided in IEC61400-3 [29]. In addition, it was assumed that the speed of the wind at the hub height varies with a resolution of 2m/s. The summary of the properties used to generate a spatiotemporal turbulent velocity field in TurbSim software [30] is shown in Table 5.

Table 5. Wind speed parameters

Normal Turbulence Model (MTN) - IEC wind class IIB	
Velocity at hub height ($\mathbf{V_{hub}}$)	2m/s – 0,7x$\mathbf{V_{ref}}$ (resolution of 2m/s)
Turbulence intensity (**I**)	14%
Power law exponent ($\boldsymbol{\alpha}$)	0.14
$\mathbf{V_{ref}}$	42.5m/s
Air density ($\boldsymbol{\rho_{ar}}$)	1.225 kg/m3
TurbModel	Kaimal spectral model

As for wave parameters, it is usual to use a joint probability distribution in order to obtain the probability of accuracy of a specific wave height associated with a wave period and wind speed. It occurs that meteoceanographic data are difficult to acquire. Therefore, based on the Campos Basin data provided in Gonçalves et al. [31], it was done an approach similar to that proposed by Zhang et al. [32]. Wave and wind were taken to be superposed independently of its directions and intensities. Thus, a lognormal distribution for wave period T_p, Eq. (1), and a Weibull distribution for H_s and V_{hub}, Eq. (2) and Eq. (3), were fitted, considering the simultaneous occurrence in the same direction for wind and wave with the same probability of occurrence.

$$P_{Tp}(T_p) = \Phi\left(\frac{ln(T_p) - b_0}{b_1}\right) \tag{1}$$

$$P_h(H_s) = 1 - \exp\left(-\left(\frac{H_s}{\alpha}\right)^{\beta}\right) \tag{2}$$

$$P_v(V_{hub}) = 1 - \exp\left(-\left(\frac{V_{hub}}{C}\right)^{k}\right) \tag{3}$$

As $P_v(V_{hub}) = P_h(H_s) = P_{Tp}(T_p)$, it is possible to calculate the wave height (H_s) and wave period (T_p) as function of the wind speed (V_{hub}). In addition, the JONSWAP spectrum was used to describe the sea state.

This methodology was chosen because it allows the investigation of the fatigue behavior as function of different wind speed and its associated wave height. It is important to note that marine current was not used, since the DLC 1.2 and DLC 6.4 consider that the current introduces an additional damping to the system, possibly reducing the damage IEC61400-3 [29]. A summary of the environmental conditions

used for the analysis is shown in Table 6.

Table 6. Environmental conditions (Gomes [19]).

Design situation	Environment State	DLC	V_{hub}	H_s	T_p	Frequency factor
			[m/s]	[m]	[s]	[-]
Operational	E1	1.2	4	3.7	11.4	8.99E-02
	E2		6	4.3	11.9	3.24E-02
	E3		8	4.8	12.4	1.28E-02
	E4		10	5.2	12.7	5.37E-03
	E5		12	5.5	13.1	2.35E-03
	E6		14	5.9	13.4	1.06E-03
	E7		16	6.1	13.7	4.92E-04
	E8		18	6.4	14	2.34E-04
	E9		20	6.7	14.2	1.13E-04
	E10		22	6.9	14.7	5.56E-05
	E11		24	7.1	14.9	2.77E-05
Parked	E12	6.4	2	2.9	10.7	8.55E-01
	E13		26	7.3	15.2	1.40E-05
	E14		28	7.5	15.4	7.16E-06

4 Structural mechanics of grouted connections

The current understanding of the structural mechanics of grouted connections is that the bending moments and shear forces due to wind and wave load are transferred from the transition piece to the monopile by means of contact pressure on the grout. Axial and torsional forces are resisted by the shear strength given by the grout to steel interface. The bending moment is the main reaction induced in OWT's and is responsible for the largest stresses and damages developed in the grout.

According to Lotsberg [33], the total bending moment transferred from the tower to the monopile is given by the summation of 4 different components. These components, as describes in Lotsberg [33] are the moment resistance due to vertical friction, horizontal friction, contact pressure and shear key. However, when the connection does not use shear key, only the first 3 equations make up the resistance of the connection against bending moment. The variables are accordingly to the geometric parameters as per Fig. 2, Fig. 3 and μ is the grout steel interface coefficient of friction; φ is the angle; k_V is the stiffness in the vertical direction for one shear key connection; δ_V is the maximum relative vertical displacement; P_{nom} is the contact pressure.

$$M_{\mu v} = 2\int_0^{\pi/2} R_p d\varphi P_{nom}\mu \frac{L_g}{2}\frac{1}{2}\left(R_p sin\varphi\right)2 \tag{4}$$

$$M_{\mu h} = 4\int_0^{\pi/2} sin\varphi R_p d\varphi P_{nom}(\varphi)\mu \frac{L_g}{2}\frac{1}{2}\left(\frac{L_g}{2}\frac{2}{3}\right)2 \tag{5}$$

$$M_p = 2\int_0^{\pi/2} sin\varphi R_p d\varphi P_{nom} \frac{L_g}{2}\frac{1}{2}\left(\frac{L_g}{2}\frac{2}{3}\right)2 \tag{6}$$

$$M_{shear} = 4\int_0^{\pi/2} k_V R_p d\varphi R_p sin\varphi(\delta_V sin\varphi) \tag{7}$$

Thus, from these equations it is possible to obtain the nominal contact pressure that is applied to the grout as a consequence of the bending (Fig. 7).

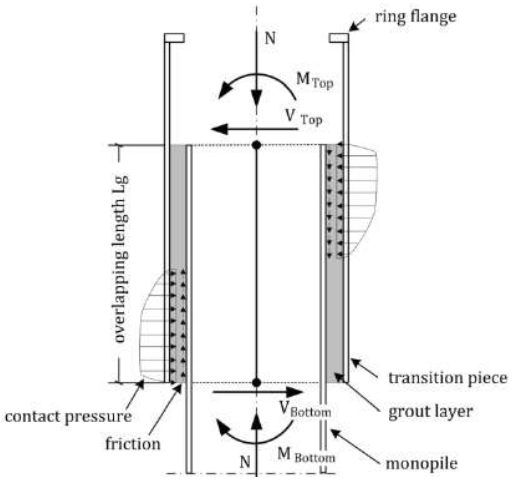

Figure 7. Reaction forces in the connection due to bending moment (Schaumann et al. [34]).

The contact pressure is calculated by Eq. (8) for conical shaped connections and by Eq (9) for cylindrical shaped connections with shear key.

$$P_{nom} = \frac{3\pi M_{Top}}{\left(R_p L_g^2(\pi + 3\mu) + 3\pi\mu R_p^2 L_g\right)} \tag{8}$$

$$P_{nom} = \frac{3\pi M_{Top}}{EL_g\left(R_p L_g^2(\pi + 3\mu) + 3\pi\mu R_p^2 L_g\right) + 18\pi^2 k_{eff} R_p^3 (\frac{R_p^2}{t_p} + \frac{R_{TP}^2}{t_{TP}})} \tag{9}$$

where E is the Young's modulus; M_{Top} is the bending moment applied on the connection which can be obtained by the global structural response from RIFLEX software [17]; and k_{eff} is the effective stiffness of the shear key, as given in Equation (10).

$$k_{eff} = \frac{2t_{TP} s_{eff}^2 nE\Psi}{4\sqrt[4]{3(1-\nu^2)}t_g^2\left\{(\frac{R_p}{t_p})^{3/2} + (\frac{R_{TP}}{t_{TP}})^{3/2}\right\}t_{TP} + ns_{eff}^2 L_g} \tag{10}$$

where $s_{eff} = s - w$ is the effective vertical distance between the shear key; ν is Poisson's ratio; n is the effective number of shear key; Ψ is the design parameter (0.5 for calculation of maximum nominal contact pressure).

The local contact pressure due to discontinuity in cross section on the top (where the connection

narrow to the transition piece) and bottom (where the connection reduces to the monopile) of the grouted joint is calculated based on a Stress Concentration Factor (SCF) provided by DNVGL-ST-0126 [12] (Equation 11).

$$FCT = 1 + 0{,}025\left(\frac{R}{t}\right)^{3/2} \tag{11}$$

When applying Equation (11), one must verify the compliance of the geometric properties of the structure. Therefore, this factor is only valid for 2250mm ≤ R ≤ 3250mm (radius of the cross section) and 50mm ≤ t ≤ 100mm (thickness of the cross section). This limitation can be best seen in Fig. 8, where the dashed lines represent the thickness limits and curves represent the radius limits of the section.

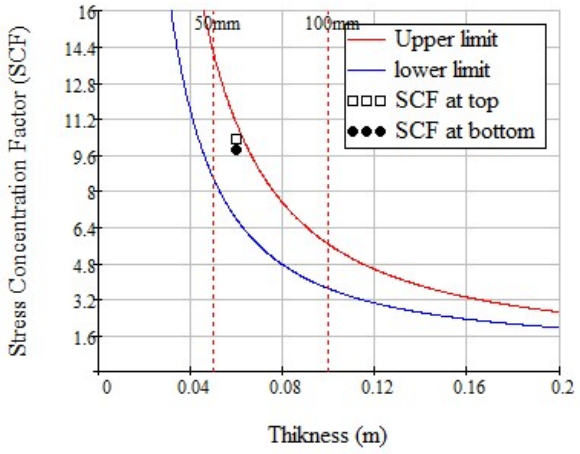

Figure 8. Stress Concentration Factor at the top and bottom of transition piece.

5 Fatigue evaluation method

Palmgren-Miner summation rule was applied in conjunction with S-N curve in order to calculate the accumulated damage. However, unlike welded joints, where the mean stress is negligible due to residual stress, the grout is strongly influenced by the mean stress load to which it is subjected. One of the ways to take this mean stress into account is the Markov Matrix method (MM), which is the method recommended by DNVGL-ST-0126 [12] and DNVGL-RP-0419 [14] to calculate fatigue in grout. In a simplified analysis, the MM consists of another way to compute the results obtained from Rainflow Counting method (RC). Instead of calculating the stress range ($\Delta\sigma$) and the number of cycles (N), the MM provides the local maximums ($\sigma_{max}, \sigma_{min}$) of each cycle and the number of cycles (N) (Fig. 9). Thus, it is possible to indirectly take the mean stress load into consideration.

In order to calculate the number of cycles to failure N, the S-N curve recommended by DNVGL-ST-C502 [35], in the compression-compression region, was chosen. This S-N curve was taken due to its conservative results when compared to other standards S-N curves as described in Gomes [19].

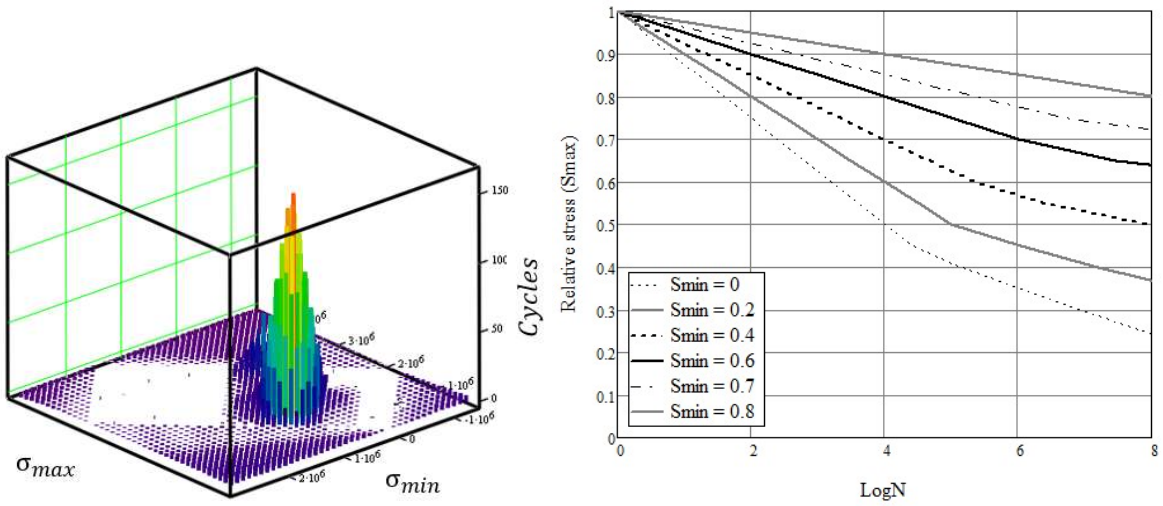

Figure 9. Left: Markov Matrix; right: S-N curve (Gomes [19]).

According to DNVGL-ST-C502 (2018) [35], the number of cycles to failure is given by Equation (11)

$$log_{10}N = C_1\left(1 - \frac{\sigma_{max}}{C_5\frac{f_{cn}}{\gamma_m}}\right)\Bigg/\left(1 - \frac{\sigma_{min}}{C_5\frac{f_{cn}}{\gamma_m}}\right) \tag{11}$$

where factor C1 is taken as 8.0 (more conservative), $\sigma_{max}, \sigma_{min}$ are the local maximum and minimum stress, γ_m is the material factor, set to 1.5 due to the thickness of the grout used and f_{cn} is the in situ compressive strength of grout, as per Equation (12).

$$f_{cn} = f_{cck}\left(1 - \frac{f_{cck}}{600}\right) \tag{12}$$

where f_{cck} is the compressive strength of the grout. In case $log_{10}N$ is greater than X, Equation (13), the fatigue life can be increased by a factor C2, given by Equation (14).

$$X = C_1\Bigg/\left(1 - \frac{\sigma_{min}}{C_5\frac{f_{cn}}{\gamma_m}}\right) + 0{,}1C_1 \tag{13}$$

$$C_2 = (1 + 0{,}2(log_{10}N - X)) \tag{14}$$

As recommended by DNVGL-ST-C502 [35], all bending moments that would introduce tensile stress in the concrete were set to $\sigma_{min} = 0$. By doing that, it is possible to analyze the grout on the compression-compression zone.

Moreover, the total simulation time for each sea state was 3.800 s, with a cut-off of 200 s in order to avoid postprocessing errors due to transient responses that arises during the turbine operation (Fig. (10)). Thus, the analysis time is in accordance with DNVGL-ST-0437 [28], which recommends a minimum simulation time of 1 hour for each sea state for more reliable results.

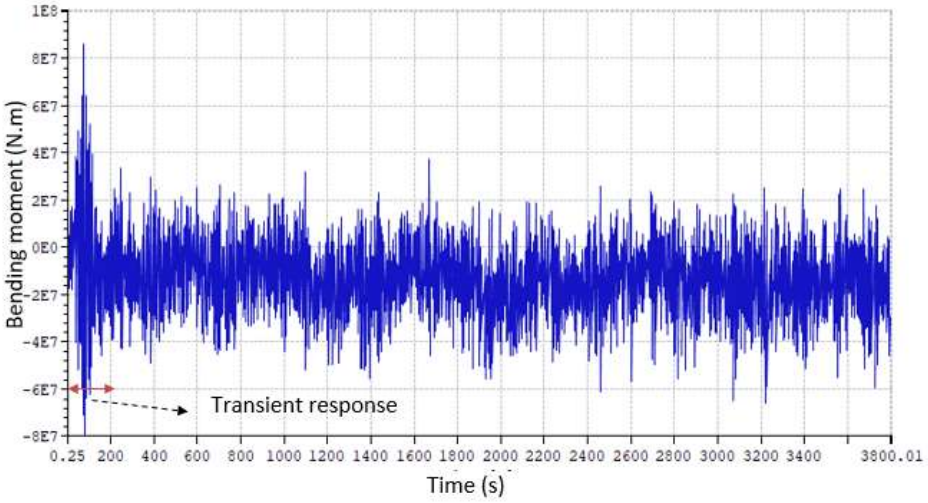

Figure 10. Bending moment time series (Gomes [19]).

6 Discussion and results

6.1 Mean load and compressive resistance effect

In order to assess the influence of the mean stress load and compressive resistance effect on fatigue damage of both shapes of connections, a set of load conditions in the operational range was taken. The compressive resistance effect was evaluated by means of changes in the mean load stress from 1 to 30 MPa, which were synthetically added to the dynamic response. The results are shown in Fig. 11.

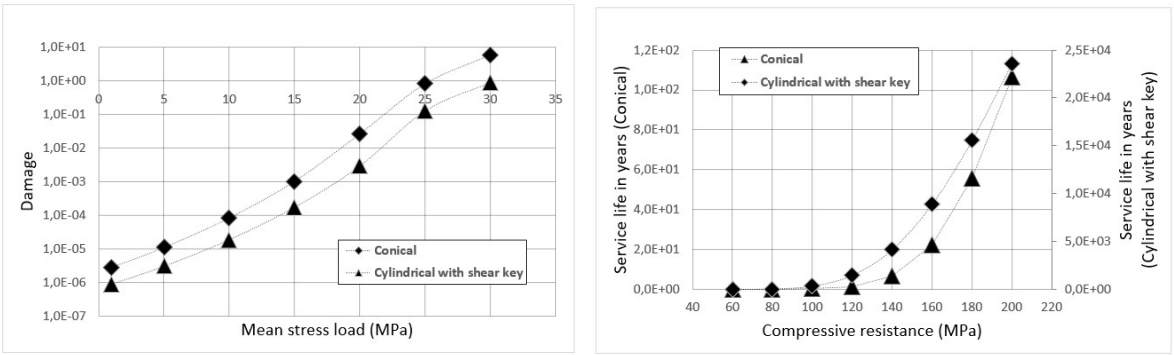

Figure 11. Left: mean load effect; right: compressive resistance effect.

It can be seen that the mean stress load has a major influence on the damage of the grout for both connections shape. However, conical shaped one presented the greatest. This mainly due to the lack of use of shear keys, which leads to a better redistribution of loads resisted by the joint. This behavior is consistent with studies presented by Schaumann et al. [34].

The redistribution of loads can be better understood by looking at the analytical Equation (9), which is used to calculate the contact pressure applied to the grout. A fraction of the total bending moment is resisted by the shear key, decreasing the loads sustain by grout. Whereas in Equation (8), used for conical shaped, the total bending moment is practically absorbed by the grout. Therefore, the stress and consequently the damage end up being higher.

Using the same time series applied in the analysis of the mean load effect, the influence of the compressive strength on the fatigue capacity of the connections were assessed. Different values for compressive strength, ranging from 60 to 200 MPa, were evaluated for each type of connection as shown

in Fig. 11. Results shows that the grout strength plays an important rule in the capacity of the conical connection than in the cylindrical one. Conical connection reached a minimum service life of 20 years just with a compressive strength of 160 MPa. While the cylindrical shaped reached a 36 years of service life with an 80 MPa grout.

The best response to grout fatigue in the cylindrical connection is in accordance with the results obtain for the mean stress load effect, which point a stress distribution due to use of shear key. Therefore, provided that the grout in the conical configuration is subjected to higher compression stresses, it is recommended the use of a grout with greater resistance for better fatigue response.

6.2 Effect of the number of shear keys

While on one hand the compressive resistance greatly affects the fatigue capacity of the conical connection, on the other hand, the number of shear key has a main effect on the cylindrical connection. This trend is shown in Fig. 12.

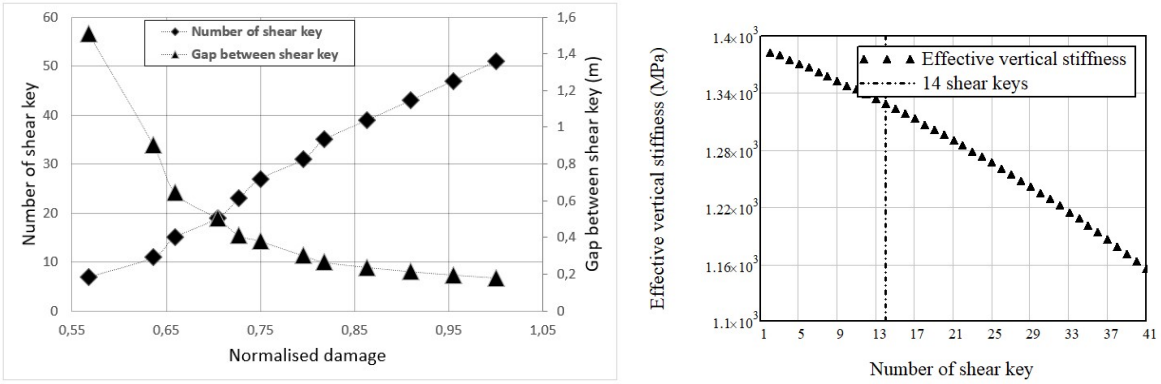

Figure 12. Left: normalized damage as function of number of shear keys; right: effective stiffness as function of number of shear keys.

The greater the number of shear key, and consequently the gap in between the shear key will be smaller, the greater the damage inflicted on grout it will be. This behavior is explained by studies conducted by Lotsberg et al. [10] and Lotsberg [33], which attributes a smaller space between the shear key to a reduction in the effective vertical stiffness, reducing the energy dissipation and, consequently, increasing the damage. This decrease in stiffness can be seen in Fig. 12, which also shows the number of shear key used in the present study (14 circumferential shear keys).

6.3 Fatigue behavior of the grouted connection

In this section, the effect of the variation of environmental states and design situation is investigated by comparing the fatigue damage of both connections. Fig 13 and Fig 14 shows the damage for each environmental state for the conical and cylindrical shaped connection for different clay soils (10 KPa, 20 KPa e 50 KPa) in which the monopile is embedded. In order to better evaluate the effects of the ES on the fatigue response, results are also shown without taking into consideration the frequency of occurrence.

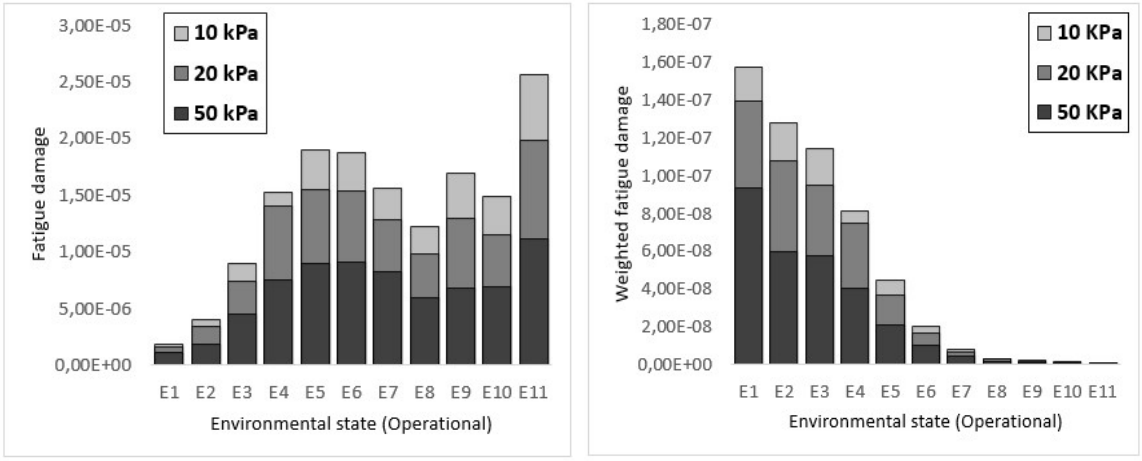

(a)

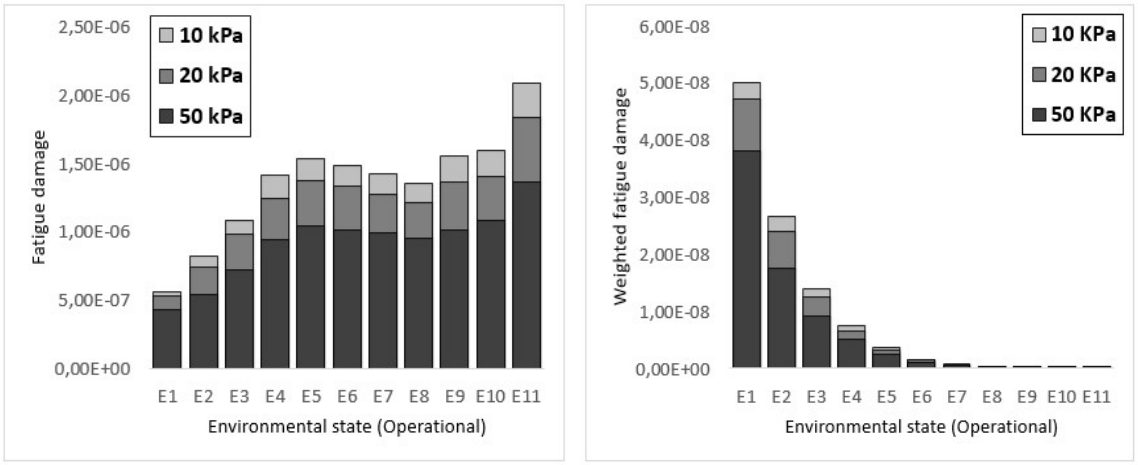

(b)

Figure 13. Damage per environmental state (operational condition): (a) conical shaped; (b) cylindrical shaped with shear key.

The fatigue behavior results, for the operational design situation, shows that increasing wind speed and wave heigth leads to greater damage, regardless of the soil type or connection shape. Yet, from E5 (V_{hub} = 12m/s and H_s = 5.0m) there is a significant change which is related to the rated power of the wind turbine. As exposed before, from wind speeds bigger than 11.4m/s the pitch control system of the blades is actvated in order to keep the rotational speed of the rotor constant. This procedure not only provides better energy yeilding, but also reduces the wind loads, leading to smaller damages to the grout connection. Though, for winds close to the cut-out limit, the wave loads seems to platy a more important rule, as the damage contribution of E11 (V_{hub} = 24m/s and H_s = 7.1m) was greater than any other state in the operational range.

However, it is important to know the frequency of occurance of each envinronmental state. As can be seen in Fig. 13, there is a complete change of the environmental state that most contributes to the structural damage. Even though, E1 (V_{hub} = 4m/s and H_s = 3.7m) was the state with lowest damage, after taking into considerantion the frequency in which this environmental state occurs, its contribution do the final damage was the greatest.

It is also possible to notice that the soils with lower undrained resistance, like 10KPa, are more susceptable to greater damages. This is not only due to the proximity of the natural frequency of the structure to the wave peak periods, but also to its proximity to the 1P frequency, what utimatily leads to dynamc amplification of the structural response. To sum up, the only difference between the conical and cylindrical shaped connections were the damage degree, as consequece of the greater loads that the grout in the conical one has to sustain due to lack of shear key.

On the other hand, when considering the non-operational (parked) design situation Fig. 14, the damage was even bigger for both connections when compared to the operational results. The support structure in clay soil with Su = 10KPa presented very high damage values, specially that produced by the environmental state E12 (V_{hub} = 2m/s, H_s = 2,9m and T_p = 10.7s) . It may be associated with the lack of aerodynamic damping, which is introduced in the structure due to operation of the wind turbine. This damping effect changes accordingly to the wind speed and it is not clear in the literature what would be its contribution to the damping ratio (ζ). However, some studies conducted by Chen and Dufour [36], Rezael et al. [37] and Gomes [19] points out values for the damping ratio ranging from 2.00-8.00%. Moreover, the higher proximity of the structure's natural frequency to the wave period peak of E12 (when compared to the others environmental states) also influenced the higher damage, increasing the amplitude of vibration, once it was less damped.

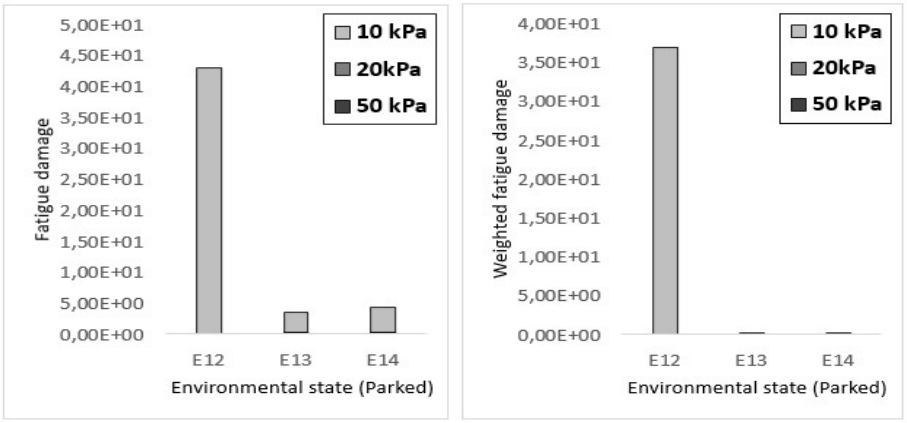

(a)

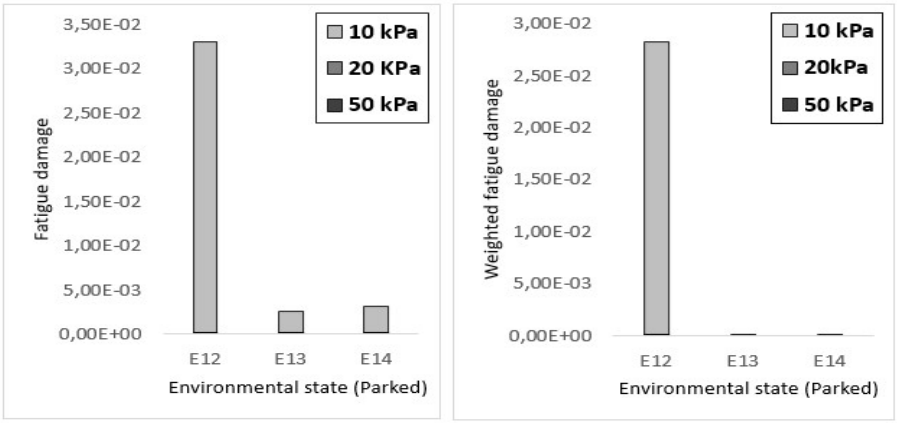

(b)

Figure 14. Damage per environmental state (parked condition): (a) conical shaped; (b) cylindrical shaped with shear key.

Finally, it is clear that the damage to the grout is small in most situations, in the order of 10^{-6}, except for the clay soil with undrained resistance of Su = 10KPa, when the turbine is in parked condition. That magnitude of damage was also obtained in the work of Wang et al. [38], which made use of the same S-N curve used in the present work.

Althoug the grout presents good resistance to fatigue due to bending moment load, this do not exclude the possibility of degradation and crack formaation that may reduce the axial capacity of the connection. This degradation can be futher analyzed using a finite element model. Though, this analysis is left as a suggestion for future work, given that it is not part of the scope of the present work.

7 Conclusion

In this work, a structural fatigue analysis of a conical shaped and a cylindrical shaped with shear key connections was performed. The structural analysis was conducted using RIFLEX software [17], where the Winkler model was implemented together with the p-y curve recommended by ANSI/API-RP-2GEO [19] and DNVGL-ST-0126 [12]. In addition, it was simulated a spatiotemporal turbulent velocity field in TurbSim software [30], which was later imported into RIFLEX software [17].

It was shown that the mean stress load and the compression strength have a great influence on the grout capacity, mainly in the conical shaped connection, because of the absense of shear key. As for the number of shear key, this also had influence on the fatigue capacity of the grout in the cylindrical one. Greater damages was noticed as the number of shear keys increased. However, better conclusions about the reasons behind it can be verified through simulation with a finite element model, which is one of the proposals for future work.

The environmental states have differents effects on the grout damage depending on the wind speed. After the rated speed it is expected a reduction on the fatigue damage as a consequence of smaller bending moments. However, up to some degree, wave loads starts to have a greater contribution to the fatigue load. This behavior is more clear when the turbine is in parked condition and no aerodynamic damping is found. As it was shown, the damage can be bigger, mainly when the natural frequency of the OWT is close to the forcing frequencies, as an example, the reponses of the OWT in clay soil with Su = 10KPa.

Acknowledgements

The work presented in this paper is the result of a partnership between Petrobras and UFRJ and was carried out with funds from the R&D from program of the Eletric Sector regulated by ANNEL, under the PD-00553-0045/2016 project, entitled “Planta Piloto de Geração Eólica Offshore”.

The authors would also like to express their gratitude to “Coordenação de Aperfeiçoamento de Nível Superior” (CAPES), for the resources destined to the production of this research.

References

[1] ABEE. Associação Brasileira de Energia Eólica. *Boletim annual de geração eólica*, 2018. Available in: http://abeeolica.org.br/. Access: July 10th of 2019.

[2] O.A.C. Amarante, D.J. Schultz, R.M. Bittencourt, N.A. Rocha, *Wind/ Hydro Complementary Seasonal Regimes in Brazil*. DEWI Magazin, v. 19, p. 79-86, 2001.

[3] A.R. Silva, F.M. Pimenta, A.T. Assireu, M.H.C. Spyrides, “*Complementary of Brazil’s hydro and offshore wind power*”, Renewable and Sustainable Energy Reviews, vol. 56, Elsevier Applied Science, pp. 413-427, 2015.

[4] I. Srikanth, S.K.R. Alluri, K. Balakrishnan, M.V.R. Murthy, M. Arockiasamy, “*Simplified Design Procedure of Monopile Foundation for Offshore Wind Turbine in Gujarat, India*”, OMAE, 61433, Trondheim, Norway, 25-30 June, 2017.

[5] EWEA. The European Wind Energy Association. *Offshore Wind in Europe: key trends and statistics*. 2017. Available in: www.ewea.org/statistics. Access: may 15th of 2018.

[6] V. Negro, J.S.L. Gutiérrez, M.D. Esteban, P. Alberdi, M. IMAZ, “*Monopiles in offshore wind: Preliminary estimate of main dimensions*”, Ocean Engineering, 133, pp. 253-261, 2017.

[7] Vattenfall. Available: https://group.vattenfall.com. Access: 24 April 2015.

[8] P. Schaumann, S. L. Lochte-Holtgreven, R. Eichstädt, T. Camp, G. Mccann, *Numerical investigation on local degradation and vertical misalignments of grouted joints in monopile foundations*, ISOPE, 23th, Alaska, USA, June 30 – July 5, 2013.

[9] C.J. Billington, G.H.G. Lewis, “*The strength of Large Diameter Grouted Connections*”, Offshore Technology Conference, OTC, Hounston, Texas.p. 291-301, 1978.

[10] I. Lotsberg, A. Serednicki, B. Håkon, L. Andreas, *Design of grouted connections for monopile offshore structures*. Stahlbau, 81(9), pp. 695-704, 2012.
[11] P. Dallyn, A. Palmeri, El-Hamalawi, R. Knight, "*Experimental testing of grouted connections for offshore substructures: a critical review*", Structures, vol. 3, pp. 90-108, 2015.
[12] DNVGL-ST-0126. *Support structures for wind turbines*. Norway: Det Norske Veritas, 2016.
[13] P. Schaumann, F. Wilke, S. Lochte-Holtgreven, "*Grout-verbindungen von monopilegründungsstrukturen– trag- und ermüdungsverhalten. Stahlbau*", vol. 77 (9). Berlin, Germany: Ernst & Sohn, 2008.
[14] DNVGL-RP-0419. *Analysis of grouted connections using the finite element method. Norway: Det Norske Veritas*, 2016.
[15] J. Jonkman, S. Butterfield, W. Musial, G. Scott, "*Definition of a 5-MW Reference Wind Turbine for Offshore System Development. Colorado*", USA: National Renewable Energy Laboratory – NREL, 2009.
[16] M. Damgaard, M. Bayat, L.V. Anderson, L.B. Ibsen, "*Assessment of the dynamic behavior of saturated soil subjected to cyclic loading from offshore monopile wind turbine foundations*", Computers and Geotechnics, vol. 61, Elsevier Applied Science, pp. 116-126, 2014.
[17] Sintef Ocean. RIFLEX 4.10.3 Theory Manual. 2017.
[18] J. Velarde, E. Bachynski, "*Design and Fatigue Analysis of Monopile Foundations to Support the 10 MW Offshore Wind Turbine*". Trondheim, Norway: Norwegian University of Science and Technology – NTNU, 2017.
[19] F. A. Gomes. "*Análise de fadiga de turbinas eólicas offshore tipo monopile com conexão grauteada*". Master theses, Federal University of Rio de Janeiro, RJ, Brazil, 2019.
[20] ANSI/API-RP-2GEO, *Petroleum and Natural Gas industries – Specific Requirements for Offshore Structures, Part 4 – Geotechnical and Foundation Design Considerations Geotechnical and Foundation Design Considerations*. Washington: American Petroleum Institute, 2011.
[21] H. Matlock, "*Correlation for design of laterally loaded piles in soft clays*". 2nd Offshore technology conference. Houston, Texas; 1970. p. 577–94, 1970.
[22] L.C. Reese, R.C. Welch, "*Lateral loading of deep foundation in clay*". J Geotech Eng, Div;101(7):633–49, 1975.
[23] T.W. Dunnavant, M.W. O'Neill, 1989, "*Experimental p–y model for submerged stiff clay*. J Geotech Eng;115(1):95–114, 1989.
[24] S. Bisoi, S. Haldar, "*Dynamic Analysis of offshore Wind Turbine in Clay Considering Soil-Monopile-Tower Interaction*", Soil Dynamics and Earthquake Engineering, vol. 63, Elsevier Applied Science, pp. 19-35, 2014.
[25] S. Schafhirt, A. Page, G.R. Eiksund, M. Muskulus, "*Influence of soil parameters on the fatigue lifetime of offshore wind turbines with monopile support structure*, Energy Procedia, vol. 94, Elsevier Applied Science, pp. 347-356, 2016.
[26] E. Smilden, E.E. Bachynski, A.J. Sørensen, "*Key Contributors to Lifetime Accumulated Fatigue Damage in an Offshore Wind Turbine Support Structure*", OMAE, 61708, Trondheim, Norway, 25-30 June, 2017.
[27] R. Gasch, J. Twele, Wind Power Plants: Fundamentals, Design, Construction and Operation, 2th ed., London: Springer, 2012.
[28] DNVGL-ST-0437 (2016). *Loads and site conditions for wind turbines*. Norway: Det Norske Veritas, 2016.
[29] IEC 61400-3. *Wind turbines – Part 3: Design requeirements for offshore wind turbines*, 2009.
[30] B. J. Jonkman and L. Kilcher. Turbsim user's guide: version 1.06.00. Draft version. National Renewable Energy Laboratory – NREL, Colorado, USA, 2012.
[31] R.T. Gonçalves, F.T. Matsumoto, B. M. Edgard, H. F. Medeiros, K. Nishimoto, "*Conceptual Design of Monocolumn Production and Storage with Dry Tree Capability*", Journal of Offshore Mechanics and Arctic Engineering, Vol. 32, November, 2010.
[32] L. Zhang, J. Zhao, X. Zhang, Q.W. Ma, "*Integrated Fatigue Load Analysis of Wave and Wind for Offshore Wind Turbine Foundations*", ISOPE, 20th, Beijing, China, June 20 – 25, 2010.
[33] I. Lotsberg, "*Structural mechanics for design of grouted connections in monopile wind turbine structures*". Marine Structures, vol. 32, Elsevier Applied Science, pp. 113-135, 2013.

[34] P. Schaumann, S. Lochte-Holtgreven, Lohaus, L., Lindschulte, N. (2010): "*Durchrutschende Grput-Verbindungen in OWEA-Tragverhalten, Instandsetzung und Optimierung*" Stahlban, Vol. 79, No. 9, pp. 637-647, Ernst & Sohn Verlag, Berlin, in German, 2010.
[35] DNVGL-ST-C502 (2018). *Offshore concrete structures*. Norway: Det Norske Veritas, 2018.
[36] C. Chen, P. Duffour, "*Modelling Damping Source in Monopile-supported Offshore Wind Turbines*", in Wind Energy, ResearchGate, 2018.
[37] R. Rezaei, P. Fromme, P. Duffour, "Fatigue Life Sensitivy of Monopile-Supported Offshore Wind Turbines to Damping", Renewable Energy, vol. 123, Elsevier Applied Science, pp. 450-459, 2018.
[38] X. Wang, T. Chen, Q. Zhao, G. Yuan, J. Liu, "*Fatigue evaluation of grouted connections under bending moment in offshore wind turbine based on ABAQUS scripting interface*". International Journal of Steel Structures, vol 16, pp. 1149-1159, 2016.